Title	Stitching interferometry for ellipsoidal x-ray mirrors
Author(s)	Yumoto, Hirokatsu; Koyama, Takahisa; Matsuyama, Satoshi et al.
Citation	Review of Scientific Instruments. 2016, 87(5), p. 051905
Version Type	VoR
URL	https://hdl.handle.net/11094/86945
rights	This article may be downloaded for personal use only. Any other use requires prior permission of the author and AIP Publishing. This article appeared in (citation of published article) and may be found at https://doi.org/10.1063/1.4950714.
Note	

Stitching interferometry for ellipsoidal x-ray mirrors

Hirokatsu Yumoto, Takahisa Koyama, Satoshi Matsuyama, Kazuto Yamauchi, and Haruhiko Ohashi

Articles you may be interested in

High-energy x-ray microbeam with total-reflection mirror optics
Rev. Sci. Instrum. **78**, 053713 (2007); 10.1063/1.2736787

At-wavelength figure metrology of hard x-ray focusing mirrors
Rev. Sci. Instrum. **77**, 063712 (2006); 10.1063/1.2216870

Relative angle determinable stitching interferometry for hard x-ray reflective optics
Rev. Sci. Instrum. **76**, 045102 (2005); 10.1063/1.1868472

Development of a Linear Stitching Interferometric System for Evaluation of Very Large X-ray Synchrotron Radiation Substrates and Mirrors
AIP Conf. Proc. **705**, 851 (2004); 10.1063/1.1757929

Microstitching interferometry for x-ray reflective optics
Rev. Sci. Instrum. **74**, 2894 (2003); 10.1063/1.1569405

Stitching interferometry for ellipsoidal x-ray mirrors

Hirokatsu Yumoto,[1,a)] Takahisa Koyama,[1] Satoshi Matsuyama,[2] Kazuto Yamauchi,[2] and Haruhiko Ohashi[1,3]

[1]*Japan Synchrotron Radiation Research Institute/SPring-8, 1-1-1 Kouto, Sayo-cho, Sayo-gun, Hyogo 679-5198, Japan*
[2]*Department of Precision Science and Technology, Graduate School of Engineering, Osaka University, 2-1 Yamada-oka, Suita, Osaka 565-0871, Japan*
[3]*RIKEN SPring-8 Center, 1-1-1 Kouto, Sayo-cho, Sayo-gun, Hyogo 679-5148, Japan*

Ellipsoidal mirrors, which can efficiently produce a two-dimensional focusing beam with a single mirror, are superior x-ray focusing optics, especially when compared to elliptical-cylinder mirrors in the Kirkpatrick–Baez geometry. However, nano-focusing ellipsoidal mirrors are not commonly used for x-ray optics because achieving the accuracy required for the surface metrology of nano-focusing ellipsoidal mirrors is difficult due to their small radius of curvature along the short ellipsoidal axis. Here, we developed a surface metrology system for nano-focusing ellipsoidal mirrors using stitching interferometric techniques. The developed system simultaneously measures sub-aperture shapes with a microscopic interferometer and the tilt angles of the sub-aperture shapes with a large Fizeau interferometer. After correcting the systematic errors included in the sub-aperture shapes, the entire mirror shape is calculated by stitching the sub-aperture shapes based on the obtained relative angles between partially overlapped sub-apertures. In this study, we developed correction methods for systematic errors in sub-aperture shapes that originated from off-axis aberrations produced in the optics of the microscopic interferometer. The systematic errors on an ellipsoidal mirror were estimated by measuring a series of tilted plane substrates and the ellipsoidal substrate. From measurements of an ellipsoidal mirror with a 3.6-mm radius of curvature at the mirror center, we obtained a measurement repeatability of 0.51 nm (root-mean-square) in an assessment area of 0.5 mm × 99.18 mm. This value satisfies the requirements for surface metrology of nano-focusing x-ray mirrors. Thus, the developed metrology system should be applicable for fabricating nano-focusing ellipsoidal mirrors. *Published by AIP Publishing.* [http://dx.doi.org/10.1063/1.4950714]

I. INTRODUCTION

Precision focusing devices are powerful tools for x-ray microscopic analyses conducted in synchrotron radiation facilities. In particular, mirror optics, which have unique characteristics such as achromaticity and high efficiency, are widely utilized as x-ray focusing devices. Precision mirror optics are manufactured using deterministic fabrication processes.[1–4] These processes use computer-controlled surface machining with nanometer accuracy for figure correction based on the surface profile. Thus, determining the surface figure of x-ray mirrors with nanometer-level accuracy is indispensable for fabricating nano-focusing x-ray mirrors.[5,6] Slope measuring profilers, as typified by long trace profilers,[7,8] and stitching interferometers[9,10] have been developed as surface profilers for x-ray mirrors. These methods have the ability to measure x-ray mirrors, including plane mirrors and elliptical-cylinder mirrors, with nanometer-level accuracy.

Two elliptical-cylinder mirrors in the crossed geometry, the so-called Kirkpatrick–Baez (K–B) geometry,[11] are generally used as two-dimensional focusing devices in x-ray microscopic analyses. Replacing the elliptical-cylinder focusing mirrors in the K–B geometry with an ellipsoidal

focusing mirror, which requires only one reflection to produce a two-dimensional focusing beam, has many advantages in terms of focusing efficiency, simple alignment, and the stability of the focusing beam size and position. In particular, ellipsoidal focusing mirrors can have a larger numerical aperture in the direction of sagittal focusing than what is possible with line-focusing mirrors in the K–B geometry. However, nano-focusing ellipsoidal mirrors have not been developed because of difficulties in the fabrication processes of two-dimensional aspherical shapes.

We have been developing nano-focusing elliptical-cylinder mirrors using stitching interferometric techniques[9,10,12,13] and ultra-precision surface finishing methods.[1,6] Compared with elliptical-cylinder mirrors, producing ellipsoidal mirrors has three major challenges: (1) metrology must be sophisticated to accurately quantify a highly sloped surface; (2) ultra-precision finishing methods must be provided to process a sloped aspheric surface; and (3) huge amounts of substrate material must be efficiently removed to form a deep concave shape. The second and third challenges regarding processing techniques have been addressed[14] in parallel with the first challenge of surface metrology addressed in this article. We refined interferometric technologies based on relative angle determinable stitching interferometry (RADSI) for measuring nano-focusing ellipsoidal mirrors in the present study. The stitching interferometric techniques developed in

a)Electronic mail: yumoto@spring8.or.jp

our previous study for measuring elliptical-cylinder mirrors have inadequate accuracy for nano-focusing ellipsoidal shapes due to the radius of curvature of a few millimeters in the short axis direction of the nano-focusing ellipsoidal mirrors. The main obstacle was that the difference profiles in the overlap area between adjacent sub-aperture shapes are too large for measuring nano-focusing ellipsoidal mirrors. Sub-aperture shapes measured using a microscopic interferometer were found to include systematic errors that originated from the small radius of curvature in the short axis direction.

The purpose of this study was to establish a surface metrology system for nano-focusing ellipsoidal mirrors. We developed correction methods for the systematic shape errors in sub-aperture measurements of nano-focusing ellipsoidal mirrors using observation results that contributed to the systematic shape errors. When the flat test surface was tilted by several milli-radians in the measurement of the microscopic interferometer, we observed that the generated systematic shape errors corresponded to the tilt angle (local slope) of a test surface with respect to the reference flat of a microscopic interferometer. This type of systematic error can be attributed to the off-axis aberrations of optical elements in the microscopic interferometer. We assumed that these errors are generated in the sub-aperture measurements of nano-focusing ellipsoidal mirrors with slope distributions of several milli-radians in the short axis direction. On the basis of the systematic shape errors evaluated by the flat surface measurement, we invented correction methods for the errors in sub-aperture measurements of nano-focusing ellipsoidal mirrors. We confirmed that a shape height of 0.42-nm root-mean-square (RMS) in a sub-aperture measurement was required for correcting the designed nano-focusing ellipsoidal mirror with a 3.6-mm radius of curvature and slope distributions of ± 74 mrad at the mirror center. A repeatability of 0.51 nm (RMS) was achieved in an assessment area of 0.5 mm × 99.18 mm with the ellipsoidal mirror; this repeatability value meets the requirements for the surface metrology of nano-focusing mirrors (<1 nm (RMS)).

II. MEASUREMENT TARGET; NANO-FOCUSING ELLIPSOIDAL MIRROR

The ellipsoidal mirror shown in Fig. 1 was designed for producing a nano-focusing beam in the hard x-ray region, which is the measurement target of the present study. The focal lengths of the mirror from the mirror center to the light source and from the mirror center to the focal point are 50 m and 0.2 m, respectively. The incidence angle at the mirror center is 9 mrad. When the reflective area on the mirror surface is 100 mm × 0.5 mm in the long and short axis directions
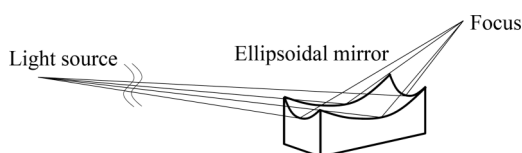
of the ellipsoid, respectively, a diffraction-limited focusing beam size of 35 nm × 60 nm full width at half maximum (FWHM) is expected at an x-ray energy of 7 keV under total reflection conditions with a platinum-coated surface. The spatial acceptance is 0.9 mm × 0.5 mm. A previous study indicated that a figure accuracy of 1 nm (RMS) is required for a nano-focusing ellipsoidal mirror to produce a diffraction-limited focusing beam using a wave-optical simulator.[15] Note that the figure error height, which generates wavefront errors corresponding to quarter wavelengths,[16] is 2.5 nm at the mirror center in these optics. Surface profilers must satisfy the measurement repeatability of less than 1 nm (RMS).

III. MEASUREMENT INSTRUMENT

A stitching interferometric technique of RADSI was applied for measuring the designed ellipsoidal mirror in this study. In the RADSI process for calculating the entire mirror shape, sub-aperture shapes are stitched based on the measured relative angles between adjacent sub-aperture shapes. The tilt angles of the sub-aperture shapes and the sub-aperture shapes are measured simultaneously. Relative angles between adjacent sub-apertures corresponding to stitching angles are calculated by the obtained tilt angles of sub-aperture shapes. This method can efficiently reduce the accumulation of stitching angle errors. The measurement instrument used in this study has approximately the same equipment layout as that developed in our previous study for measuring nano-focusing elliptical-cylinder mirrors.[12,13] Fig. 2 shows the measurement instrument. In the present system, sub-aperture shapes are measured using a white-light microscopic interferometer (ZYGO, NewView 7300), and the tilt angles of the sub-aperture shapes are measured using a 6-in. Fizeau interferometer (ZYGO, VeriFire XP/D). Test mirrors are scanned and measured along the same stitching direction in the longitudinal direction of the x-ray mirrors. Every sub-aperture shape is measured at the same focus position based on white-light interference conditions in order to prevent changes in the systematic errors due to defocus errors. Compared to the previous study, the instrument for measuring ellipsoidal mirrors in the present study has several major changes, including new interferometers, improved stiffness of the stages

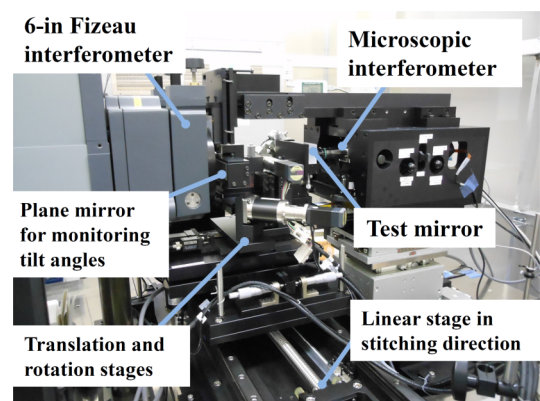FIG. 1. Diagram of an ellipsoidal focusing mirror.

FIG. 2. Photograph of the measurement instrument.

under the microscopic interferometer, and the addition of a rotation stage around the long axis of the ellipsoidal mirrors.

In the designed mirror, sub-aperture shapes were measured with a Mirau objective (20×) and a zoom lens (0.5×). The field of view was 707 μm × 530 μm. The spatial sampling using a camera with 640 × 480 array was 1.1 μm. The objective had a spatial resolution of 0.87 μm, which is calculated by the Rayleigh criterion of 0.61$\lambda/N.A.$,[17] where λ is the wavelength of light (570 nm) and $N.A.$ is the numerical aperture (0.4).

IV. ESTIMATION OF SYSTEMATIC SHAPE ERRORS

A. Surface profile and slope distribution in the sub-aperture shape

The designed ellipsoidal mirror was used for the assessment in this study. This mirror had a figure error height of several hundred nanometers along the long axis direction after fabrication with a computer-controlled grinding process.[14] The surface profile of the mirror was measured with the microscopic interferometer. Fig. 3(a) shows the obtained sub-aperture shape, and an interference fringe pattern was observed as shown in Fig. 3(b). At the edge in the short axis direction, the height difference between adjacent pixels was 80 nm. At this point, the surface had a slope of 70 mrad. This slope was comparable to the maximum slope, which is measurable with the mentioned interferometer's configuration. The designed mirror has a radius of curvature from 29 to 62 m and from 3.1 to 4.0 mm in the long and short axis directions, respectively. The depth of the mirror along 100 mm in the long axis direction is 29 μm. The incident angle distribution is ±1.1 mrad along 100 mm in the long axis direction. In the sub-aperture area at the mirror center, the depth along 700 μm in the long axis direction is 1.4 nm, whereas the depth along 500 μm in the short axis direction is 9 μm. As described above, the designed mirror has a large slope distribution in the short axis direction compared to that in the long axis direction. In this study, we mainly consider

the systematic errors generated in the measurement condition in which a test surface is tilted in the short axis direction toward the reference flat of the interferometer. Off-axis illumination by a reflected light from the tilted surface will produce off-axis aberrations such as coma and astigmatism.

B. Observation of systematic shape errors using a flat surface

We observed the systematic errors caused by off-axis aberrations using a test substrate with a flat surface. The above-mentioned measurement conditions were used with an assessment area of 707 μm × 530 μm by the optical elements. The test substrate was measured under conditions with different tilt angles around the long axis direction. This angle corresponded to the slope of an ellipsoidal mirror in the short axis direction. In this case, a 0-mrad condition corresponds to a null fringe condition in which the test substrate was measured in parallel with the reference flat of the interferometer. The measured profiles were compared to the 0-mrad condition. Difference profiles, which show the systematic shape errors, were calculated. Fig. 4(a) shows the difference profiles against the tilt angles. Fig. 4(b) shows a

FIG. 4. Observed systematic errors in measurements of tilted flat surface. (a) Difference profiles against the tilt angles. Difference profiles were calculated by subtracting a profile measured in the 0-mrad condition from a profile measured at each tilt angle. (b) Relationship between the tilt angle and the RMS error height of the difference profiles.
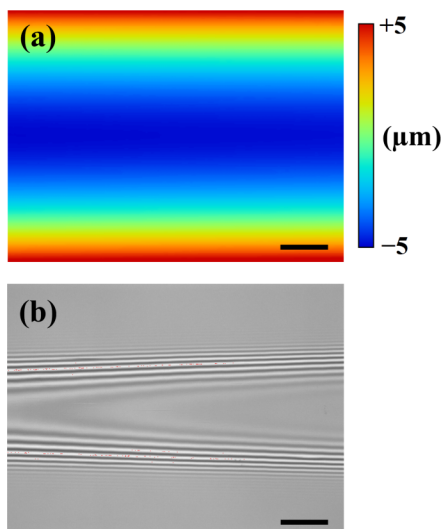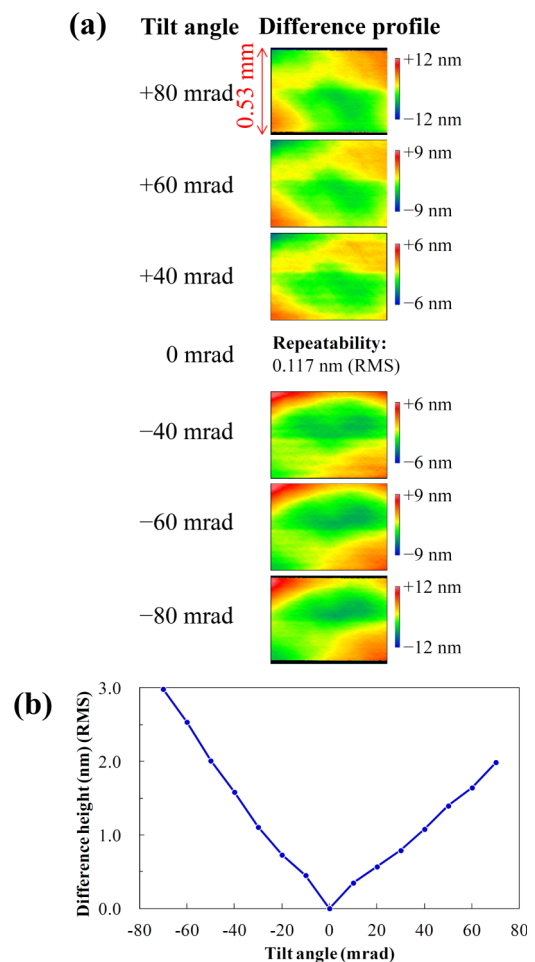
FIG. 3. Surface profile (a) and interference fringe pattern (b) of an ellipsoidal object measured with a microscopic interferometer. The scale bars are 100 μm.

relationship between the tilt angle and the RMS error height of the difference profiles. A measurement repeatability of 0.2 nm (RMS) was obtained at each tilt angle. As shown in Fig. 4, the RMS error height increased with the increasing tilt angle, while the shape of the difference profiles remained almost unchanged. We confirmed that the systematic errors are generated corresponding to the tilt angle.

C. Approximate representation of systematic shape errors in the measurement of the tilted flat surface

On the basis of the observed results, we considered a method for expressing the systematic shape errors generated in the measurement of the tilted flat object. Zernike polynomials[18] were used for fitting the difference profiles. We expected that the systematic shape errors caused by the off-axis aberrations could be expressed using a few low-order Zernike polynomial terms, which are commonly applied for expressing optical aberrations. However, many terms were required for representing the errors as described below. For the difference profile measured in the −60-mrad condition, Fig. 5 shows the relationship between the residual height of the difference profile after the polynomial fitting and term numbers of used polynomials. About 70 terms were required for fitting the difference profile to reduce the residual height to less than 0.3 nm (RMS).

Fittings using Zernike polynomials were conducted for difference profiles obtained at each tilt angle condition. Fig. 6 shows a relationship between the tilt angle and the Zernike expansion coefficients. Only the term numbers from 3 to 11 are shown in Fig. 6, while about 70 terms were calculated. The coefficient of each term is continuously distributed against the tilt angle. The systematic shape errors for a tilted flat surface can be calculated by interpolating the results for any tilt angle.

D. Expression of systematic shape errors in the ellipsoidal surface measurement

The purpose in correcting the sub-aperture shape is to minimize the difference shape, which is systematically caused by the measurement of a curved surface, between stitching sub-aperture shapes in the measurement of ellipsoidal mirrors. We developed a method for calculating plausible systematic shape errors in the sub-aperture shapes. Calculation procedures are explained in detail below. The procedures
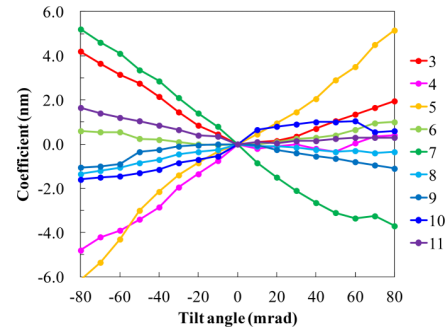
FIG. 6. Relationship between tilt angles and Zernike expansion coefficients.

can be summarized as follows. Systematic shape errors on a curved shape $C(i, j)$ (to be described) were estimated based on the observed systematic shape errors on the tilted flat shape $F(i, j, S(i, j))$ (to be described). Moreover, adequate corrections for $C(i, j)$ were introduced. Then, the systematic shape errors on the ellipsoidal mirror $E(i, j)$ (to be described) were finally expressed.

In the measurement of a microscopic interferometer, the difference of the wave front, which is an optical path difference, between the reflected light from the reference flat and the reflected light from the test surface is eventually observed as a shape. When the reflected light from the tilted surface is returned to the optics of the interferometer, it passes through a different optical path than the incident light. This results in the generation of an optical path difference and is measured as systematic shape errors. Wavefront errors generated by off-axis illumination are due to inherent imperfections of an optical system of interferometers. By expressing the systematic shape errors included in the measurement of the tilted test surface as described below, the expression of the systematic shape errors in the profile of a tilted flat surface is expanded to systematic shape errors in the profiles of the ellipsoidal surface.

In measurements of the tilted flat object, the height of the observed systematic shape error is expressed as $F(i, j, S(i, j))$ with variables of position (i, j) (pixel number) along the short and long axis directions, respectively, and a local slope $S(i, j)$ at the measurement position (i, j). When a tilted flat surface is measured, the local slope $S(i, j)$ corresponds to the tilt angle of the substrate at every position (i, j). In this case, $S(i, j)$ is constant. As mentioned before, $F(i, j, S(i, j))$ is a measurable value and was expressed using Zernike polynomials. When $\Delta F(i, j, S(i, j))$ is defined as half of the difference between the height of the systematic shape error at the next position (i, j), $\Delta F(i, j, S(i, j))$ is expressed as follows:

$$\Delta F(i, j, S(i, j)) = 0.5[F(i + 1, j, S(i + 1, j)) - F(i - 1, j, S(i - 1, j))]. \tag{1}$$

Then, $F(i, j, S(i, j))$ can be approximately expressed with a summation operation:

$$F(i, j, S(i, j)) = \sum_{k=0}^{i-1} \Delta F(k, j, S(k, j)). \tag{2}$$

In this expression, it can be assumed that the systematic shape errors are the result of integrated local wave-front errors (systematic shape errors) produced by a local slope.
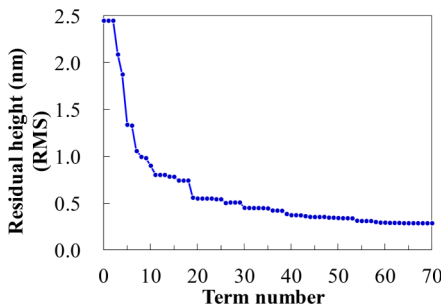

FIG. 5. Relationship between the residual height of the difference profile after the polynomial fitting and term numbers of used polynomials. The difference profile was measured in the −60 mrad condition. Residual height in RMS was calculated in an area of 707 μm × 508 μm.

As a basic assumption in the measurement of an ellipsoidal mirror, we assumed that systematic shape errors for curved surfaces are also a result of integrated local wave-front errors produced by the local slope. When an ellipsoidal surface is measured, $S(i,j)$ is not constant for every position (i,j). The slope changes along the short axis direction of an ellipsoidal mirror. At first, we assumed that the height of the systematic shape error in the sub-aperture shapes is zero at the lowest point of an ellipsoidal shape along the short axis direction. Note that this is not a reasonable assumption as described later. (See the last sentence of Section IV D.) Then, the height of the systematic shape error for a curved substrate $C(i,j)$ is similarly calculated using Equation (2). In this case, $S(i,j)$ was calculated from a measured surface profile and is not an independent variable in $C(i,j)$.

The systematic shape error, $E(i,j)$, in the sub-aperture shape of the ellipsoidal mirror was approximately expressed using simple mathematical formulas to minimize overlap errors with utilizing the above calculated error, $C(i,j)$, because $C(i,j)$ required additional corrections. As a result, the following equation was employed for the ellipsoidal mirror:

$$E(i,j) = C(i,j) \cdot (1 + Pr/R) + \xi(i,j), \qquad (3)$$

where R (m) is the radius of curvature of the measured shape, Pr is a constant calculated as -2.219×10^{-3}, and $\xi(i,j)$ is a two-dimensional height map. Fig. 7 shows the calculated $E(i,j)$ (Fig. 7(a)) at the center of the designed ellipsoidal mirror and an estimated $\xi(i,j)$ (Fig. 7(b)). Here, $E(i,j)$ has RMS height of 0.42 nm, which depends on a radius of curvature and slope distributions of the measured shape. Several nanometer heights were required to correct the systematic error in the sub-aperture area with a depth of 9 μm and slope distributions of ±74 mrad in the short axis direction. As shown in Fig. 7(a), the calculated systematic shape error in

the sub-aperture shape has nonzero values at the lowest point of the ellipsoidal shape along the short axis direction.

V. STITCHING PROCEDURES

Before stitching the sub-aperture shapes, the measured sub-aperture shapes were corrected to reduce systematic errors according to the following processes. First, the shape of the reference flat was subtracted from the sub-aperture shapes. This shape was evaluated by averaging the profiles of a smooth and flat object. Second, a correction was performed for eliminating the systematic shape errors caused by the tilted shape along the long axis direction. These errors were expressed as a parabolic curve as a function of the tilt angle along the long axis of the measured surface based on evaluated results. At the maximum tilt angle of 1 mrad, the correction shape had a depth of 0.3 nm along a length of 700 μm. Third, the above described corrections were performed for eliminating systematic shape errors caused by the curved shaped in the short axis direction. Fourth, the in-plane rotation error in alignment between the position of the interferometer head and the stitching direction (the direction of scanning stage movement) was corrected as a constant value. Finally, the pixel length was adjusted to the need of measurements. In this study, a central area of 700 μm $\times$ 500 μm was selected with a pixel length of 10 μm. Then, the sub-aperture shapes were stitched based on the measured relative angles between sub-aperture shapes for both the long and short axis directions. The stitching height was calculated to minimize overlap errors between sub-aperture shapes.

VI. MEASUREMENT REPEATABILITY

The designed ellipsoidal mirror was measured with the developed instrument under the following conditions. The mirror substrate was made of synthetic silica glass and was initially uncoated. The substrate size was 100 mm $\times$ 50 mm $\times$ 30 mm (thickness). The evaluated area of the mirror was 99.18 mm $\times$ 0.5 mm in the long and short axis directions, respectively. The measured interval of the sub-aperture shapes was 0.5 mm in the stitching direction, which is the same as the long axis direction of the ellipsoid. The field of view of the microscopic interferometer was 707 μm $\times$ 530 μm in the long and short axis directions, respectively. A total of 198 sub-aperture shapes were stitched. The measurement time for 198 sub-apertures was 2 h. As a result of the above-mentioned stitching procedures, the obtained overlap errors were less than 0.2 nm (RMS) on average, which is sufficient for fabricating x-ray mirrors. At the time of the evaluation, this mirror was estimated to have a figure error height of 3 nm (RMS). This mirror was fabricated using a computer-controlled process[14] with an area of 0.5 mm $\times$ 95 mm.

To assess the measurement repeatability, four measurements were performed 30 h after placing the substrate on the instrument. Fig. 8 shows the obtained repeatability, which was evaluated using a difference shape from the averaged shape. Fig. 8(a) shows one of the two-dimensional measurement repeatability evaluation results. Fig. 8(b) shows a
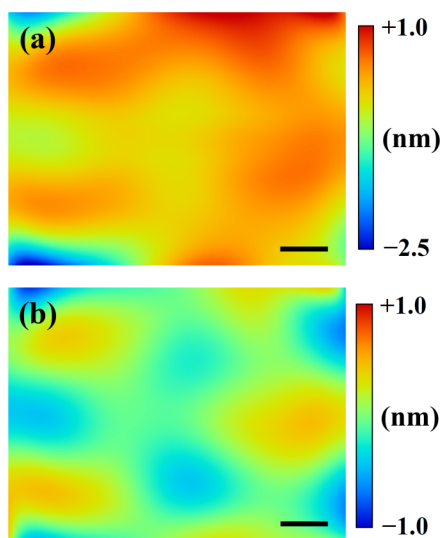

FIG. 7. Estimated systematic shape errors in a sub-aperture shape at the center of the designed ellipsoidal mirror measured with a microscopic interferometer. Height map (a) depends on a radius of curvature of the measured shape. Height map (b) is independent of a radius of curvature of the measured shape. The scale bars are 100 μm.
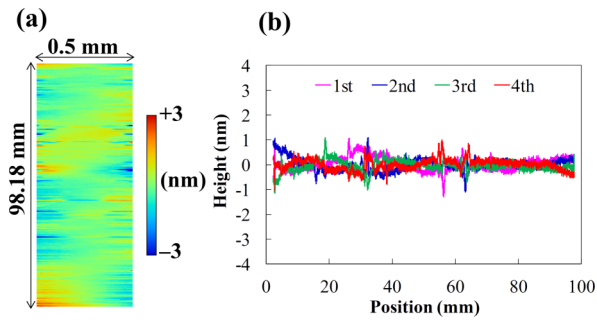
(a)   **(b)**

FIG. 8. Measurement repeatability. (a) One of the two-dimensional evaluation results. (b) A cross-sectional profile of the two-dimensional evaluation results in the long axis direction along the mirror center.
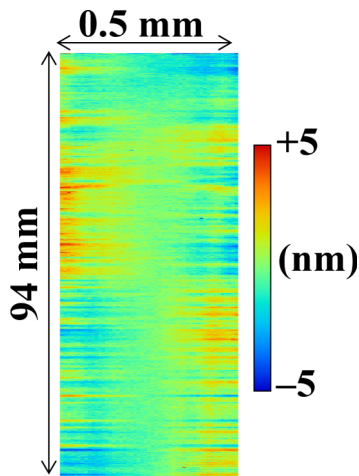

FIG. 9. Difference profile of the results obtained before and after platinum coating.

cross-sectional profile of the two-dimensional evaluation results in the long axis direction along the mirror center. We achieved an average measurement repeatability of 0.51 nm (RMS) at the two-dimensional area and 0.28 nm (RMS) along the center line.

In addition, the surface shape was compared to the surface after platinum coating of 50 nm in thickness. Four measurement results were averaged to determine the surface profiles. Fig. 9 shows a difference profile between the results obtained before and after platinum coating. A difference height of 0.98 nm (RMS) was reproduced in an assessment area of 0.5 mm × 94 mm. This low difference height indicates measurement precision after resetting the substrate, which included coating errors of platinum. Under the existing conditions, the main factor in measurement errors is considered to be a result of minute position errors occurring between sub-aperture shapes, which are associated with motion errors of the translation stage in the stitching direction. The pitching motion error of the stage generates rotation errors in the surface plane of the test mirror.

VII. SUMMARY AND CONCLUSION

We described a surface profiler developed based on a precision stitching interferometer for the purpose of fabricating nano-focusing ellipsoidal mirrors. Correction methods for systematic shape errors in the sub-aperture shapes were invented for measuring ellipsoidal mirrors with the microscopic interferometer. The evaluated results of the measurement repeatability of 0.51 nm (RMS) meet the targeted measurement requirement of less than 1 nm (RMS) for the surface profiler of the ellipsoidal mirror. Thus, the developed metrology system should be applicable for fabricating nano-focusing ellipsoidal mirrors. The results of fabrications of the nano-focusing ellipsoidal mirror with the developed metrology system will be reported in the near future.

[1] K. Yamauchi, H. Mimura, K. Inagaki, and Y. Mori, Rev. Sci. Instrum. **73**, 4028 (2002).
[2] W. Liu, G. E. Ice, J. Z. Tischler, A. Khounsary, C. Liu, L. Assoufid, and A. T. Macrander, Rev. Sci. Instrum. **76**, 113701 (2005).
[3] J. E. DeGroote, A. E. Marino, J. P. Wilson, A. L. Bishop, J. C. Lambropoulos, and S. D. Jacobs, Appl. Opt. **46**, 7927 (2007).
[4] T. Arnold, G. Böhm, R. Fechner, J. Meister, A. Nickel, F. Frost, T. Hänsel, and A. Schindler, Nucl. Instrum. Methods Phys. Res., A **616**, 147 (2010).
[5] H. Mimura, S. Handa, T. Kimura, H. Yumoto, D. Yamakawa, H. Yokoyama, S. Matsuyama, K. Inagaki, K. Yamamura, Y. Sano, K. Tamasaku, Y. Nishino, M. Yabashi, T. Ishikawa, and K. Yamauchi, Nat. Phys. **6**, 122 (2010).
[6] K. Yamauchi, H. Mimura, Takashi Kimura, H. Yumoto, S. Handa, S. Matsuyama, K. Arima, Y. Sano, K. Yamamura, K. Inagaki, H. Nakamori, J. Kim, K. Tamasaku, Y. Nishino, M. Yabashi, and T. Ishikawa, J. Phys.: Condens. Matter **23**, 394206 (2011).
[7] S. Qian, W. Jark, and P. Z. Takacs, Rev. Sci. Instrum. **66**, 2562 (1995).
[8] P. Z. Takacs, E. L. Church, C. J. Bresloff, and L. Assoufid, Appl. Opt. **38**, 5468 (1999).
[9] K. Yamauchi, K. Yamamura, H. Mimura, Y. Sano, A. Saito, K. Ueno, K. Endo, A. Souvorov, M. Yabashi, K. Tamasaku, T. Ishikawa, and Y. Mori, Rev. Sci. Instrum. **74**, 2894 (2003).
[10] H. Mimura, H. Yumoto, S. Matsuyama, K. Yamamura, Y. Sano, K. Ueno, K. Endo, Y. Mori, M. Yabashi, K. Tamasaku, Y. Nishino, T. Ishikawa, and K. Yamauchi, Rev. Sci. Instrum. **76**, 045102 (2005).
[11] P. Kirkpatrick and A. V. Baez, J. Opt. Soc. Am. **38**, 766 (1948).
[12] H. Yumoto, H. Mimura, T. Kimura, S. Handa, S. Matsuyama, Y. Sano, and K. Yamauchi, Surf. Interface Anal. **40**, 1023 (2008).
[13] H. Yumoto, H. Mimura, S. Handa, T. Kimura, S. Matsuyama, Y. Sano, H. Ohashi, K. Yamauchi, and T. Ishikawa, Nucl. Instrum. Methods Phys. Res., A **616**, 203 (2010).
[14] H. Yumoto, T. Koyama, S. Matsuyama, K. Yamauchi, and H. Ohashi, Proc. SPIE **9206**, 920605 (2014).
[15] H. Yumoto, T. Koyama, S. Matsuyama, K. Yamauchi, and H. Ohashi, AIP Conf. Proc. **1696**, 020033 (2016).
[16] M. Born and E. Wolf, *Principles of Optics*, 7th ed. (Cambridge University Press, Cambridge, 2001), p. 528.
[17] M. Born and E. Wolf, *Principles of Optics*, 7th ed. (Cambridge University Press, Cambridge, 2001), pp. 371 and 462.
[18] M. Born and E. Wolf, *Principles of Optics*, 7th ed. (Cambridge University Press, Cambridge, 2001), pp. 523–525.